Spin Electronics

Controllable Reset Behavior in Domain Wall–Magnetic Tunnel Junction Artificial Neurons for Task-Adaptable Computation

Samuel Liu^{1* (1)}, Christopher H. Bennett^{2** (1)}, Joseph S. Friedman^{3*** (1)}, Matthew J. Marinella^{2*** (1)}, David Paydarfar⁴, and Jean Anne C. Incorvia^{1** (1)}

- ¹Department of Electrical and Computer Engineering, The University of Texas at Austin, Austin, TX 78712, USA
- ² Sandia National Laboratories, Albuquerque, NM 87123, USA
- ³Department of Electrical and Computer Engineering, The University of Texas at Dallas, Richardson, TX 75080, USA
- ⁴Department of Neurology, The University of Texas at Austin, Austin, TX 78712, USA
- * Student Member, IEEE
- ** Member, IEEE
- *** Senior Member, IEEE

Received 5 Mar 2021, accepted 14 Mar 2021, published 30 Mar 2021, current version 28 Apr 2021.

Abstract—Neuromorphic computing with spintronic devices has been of interest due to the limitations of CMOS-driven von Neumann computing. Domain wall—magnetic tunnel junction (DW-MTJ) devices have been shown to be able to intrinsically capture biological neuron behavior. Edgy-relaxed behavior, where a frequently firing neuron experiences a lower action potential threshold, may provide additional artificial neuronal functionality when executing repeated tasks. In this letter, we demonstrate that this behavior can be implemented in DW-MTJ artificial neurons via three alternative mechanisms: shape anisotropy, magnetic field, and current-driven soft reset. Using micromagnetics and analytical device modeling to classify the Optdigits handwritten digit dataset, we show that edgy-relaxed behavior improves both classification accuracy and classification rate for ordered datasets while sacrificing little to no accuracy for a randomized dataset. This letter establishes methods by which artificial spintronic neurons can be flexibly adapted to datasets.

Index Terms—Spin electronics, domain wall dynamics, magnetic logic devices, magnetic tunnel junctions, neuromorphic computing.

I. INTRODUCTION

Within the past decade, rapid growth in data volume and complexity has accelerated the need for alternatives to CMOS-driven von Neumann architecture that has dominated modern computing. Contemporary data-intensive tasks often expose the problem of a memory wall, where computation and memory are separate and processes are executed sequentially [Wulf 1995]. This leads to significant delay and energy consumption, particularly in prediction, interpolation, and extrapolation tasks that deal with complex sets of data. Due to these difficulties, research efforts have been directed toward eliminating these bottlenecks through neuromorphic computing, which draws inspiration from the parallel processing and efficiency of biological neural systems, e.g., the human brain. Hardware implementation of neuromorphic computing requires the development of artificial structures analogous to biological systems: neurons that are interconnected through synaptic weights. Artificial neural networks (ANNs) have the potential to overcome limitations faced by von Neumann computing [Furber 2016].

A fundamental building block of an ANN is the artificial integrateand-fire (**IF**) neuron [Burkitt 2006]. A biological neuron receives impulses from other neurons through a synaptic network and builds up a membrane potential (integration). When this membrane potential reaches a threshold, the neuron generates an action potential, or a voltage spike, which then propagates to other connected neurons in rons incorporate the tendency of biological neurons to gradually lose membrane potential (leak) after a period without stimulation [Nahmias 2013, Hassan 2018, Cui 2020].

An additional behavior of many biological neurons, for example,

the network (firing). Furthermore, leaky integrate-and-fire (LIF) neu-

An additional behavior of many biological neurons, for example, mammalian pyramidal neurons in the cortex and hippocampus, is a transition between edgy and relaxed states. Consequently, the depolarizing shift causes the cell to be at a lower threshold for generating additional action potentials (edgy), whereas a neuron that does not fire often requires a higher threshold to generate an action potential (relaxed). This phenomenon, called afterdepolarization, is an important mechanism underlying neural oscillations associated with information processing and rhythmic motor functions in the mammalian central nervous system [Llinás 1988, Bean 2007]. This edgy-relaxed behavior can be beneficial for artificial neurons that are used for datasets that have a degree of repetitive order.

A promising candidate in implementing artificial neurons is the domain wall–magnetic tunnel junction (**DW-MTJ**) device [Currivan 2012, Currivan-Incorvia 2016, Alamdar 2021], which consists of a perpendicularly magnetized ferromagnetic (**FM**) track containing a single DW and a sensing MTJ consisting of a fixed FM layer separated from the track by a thin insulating layer (Fig. 1). The DW propagates along \hat{x} when a current is applied across the DW track through spin transfer torque. If a heavy metal layer is introduced, the DW can also be propagated through SOT. The position of the DW represents the integration of the artificial neuron. The distance between the starting position of the DW and the sensing MTJ represents the firing threshold of the artificial neuron; as the DW passes underneath the sensing MTJ,

Corresponding author: Samuel Liu (e-mail: liukts@utexas.edu). Digital Object Identifier 10.1109/LMAG.2021.3069666

1949-307X © 2021 IEEE. Personal use is permitted, but republication/redistribution requires IEEE permission.

See https://www.ieee.org/publications/rights/index.html for more information.

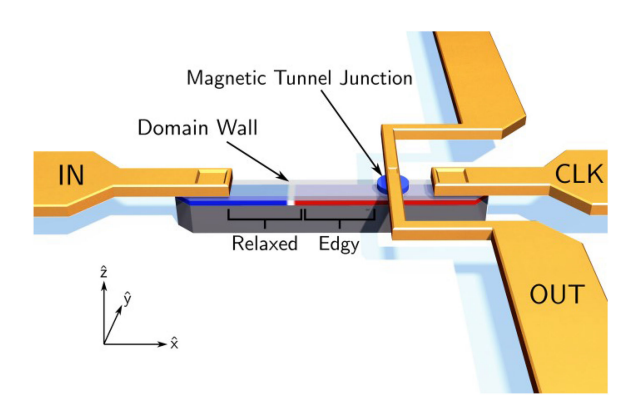


Fig. 1. Schematic of the DW-MTJ device. The red and blue in the CoFeB FM layer represent domains of antiparallel magnetization in \hat{z} . The white boundary represents the DW. The sensing MTJ is depicted as a blue disk aligned close to the right end of the track. The translucent layer represents the MgO insulating layer. The dark gray bottom layer depicts an optional heavy metal layer for SOT propagation. Generalized boundaries of edgy-relaxed states are also indicated.

a resistance change occurs, causing a spike in output current. This output spike then triggers a reset current that is applied in the opposite direction to integration, propagating the DW back to the initial position in preparation for the next integration. The DW-MTJ device has been shown to implement IF behavior and exhibit energy efficiency both on the device and circuit levels [Sharad 2012, Sengupta 2016].

In a DW-MTJ neuron, the DW is typically reset to the initial position after firing, which will be referred to as a hard reset. Edgy-relaxed behavior can be implemented in a DW-MTJ neuron by not completely resetting the DW to the initial position, leading to a higher integration state for a neuron that has recently fired; this will be referred to as a soft reset. This can be accomplished by manipulating shape anisotropy, external magnetic field, and reset current. Shape anisotropy and external magnetic field have already been shown to leaking behavior by moving the DW backward in DW-MTJs [Brigner 2019]. This can be adapted for edgy-relaxed behavior by not resetting the neuron after firing, and instead allowing the DW to propagate backward for a duration of time before integration begins again. The distinction between leaking behavior and edgy-relaxed behavior is that leaking behavior describes action potential during integration, whereas edgy-relaxed behavior is dictated by neuron behavior in between rounds of integration. If the time duration and the leaking velocity of the DW are tuned to partially reset the neuron, the result is that the recently fired neuron has a lower firing threshold than the other neurons in the layer. The application of a soft reset current is similar in that by reducing the magnitude of the reverse polarity current compared to a hard reset, the same effect can be realized.

In this letter, we show using micromagnetic simulations and analytical modeling that by taking advantage of shape anisotropy and magnetic field to implement inherent edgy-relaxed behavior in DW-MTJ neurons, the delay and classification accuracy of an ANN is improved on data with repetitive inputs while sacrificing little to no accuracy for a completely randomized dataset. We also show that tuning the reset signal to implement edgy-relaxed behavior can result in delay and classification accuracy improvements. A comparison of the benefits of each method is also presented.

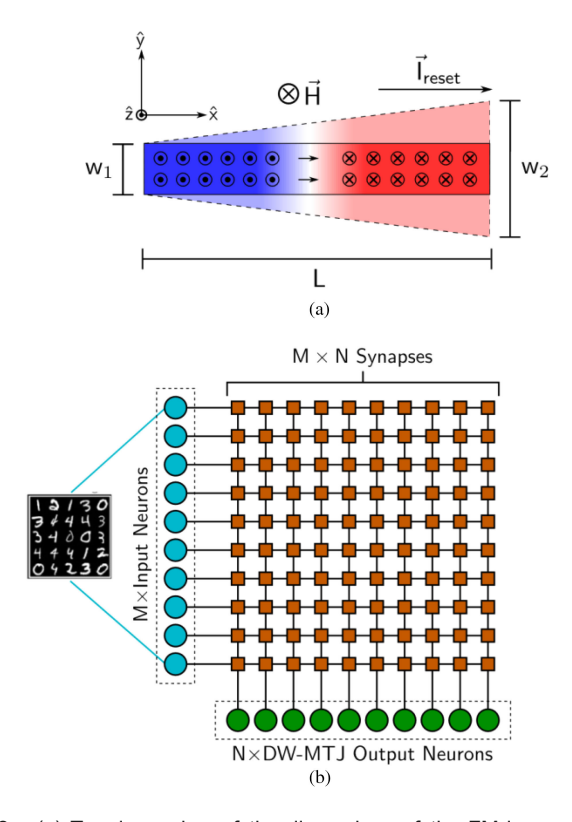


Fig. 2. (a) Top-down view of the dimensions of the FM layer of the DW-MTJ neuron. The DW is depicted in white. The soft reset methods using magnetic field (\vec{H}) , shape anisotropy (W_1,W_2,L) , and reset current $(\overrightarrow{I_{\text{reset}}})$ are also shown. (b) Diagram of perceptron depicting input neurons and data, synapse network, and the simulated DW-MTJ output neurons. For Optdigits classification, there are 64 input neurons and ten output neurons.

II. METHODS

A. Single-Device Micromagnetics Model

To demonstrate the ability of a DW-MTJ neuron to implement edgy-relaxed behavior, an FM track containing a single DW is modeled using MuMax3 micromagnetics simulation software that solves the Landau–Lifshitz–Gilbert equation [Vansteenkiste 2014]. We study the edgy-relaxed behavior for three possible leaking methods: magnetic field, shape-anisotropy, and reset current, as defined in Fig. 2. These reset options are compared against a DW-MTJ IF neuron with a hard reset, which will be referred to as the baseline neuron.

A rectangular wire of dimensions $W_1 = W_2 = 50$ nm, L = 250 nm, and t = 1.5 nm is simulated for the field-driven and current-driven reset methods. For shape-anisotropy-driven reset, a trapezoidal wire is simulated with dimensions 25 nm \times 100 nm \times 250 nm \times 1.5 nm for $W_1 \times W_2 \times L \times$ thickness t, where W_1, W_2 , and L are defined in Fig. 2(a), similar to the model described in Brigner [2019]. The mesh size of the simulation was chosen to be 1 nm \times 1 nm \times 1.5 nm. For field-driven reset, an additional external field $\vec{H} = 400$ A/m is applied. The material parameters chosen are those of CoFeB: exchange stiffness $A_{\rm ex} = 1.3 \times 10^{-11}$ J/m, saturation magnetization $M_{\rm sat} = 0.8 \times 10^6$ A/m, uniaxial magneto-crystalline anisotropy in $\hat{z} K_{\rm u} = 5 \times 10^5$ J/m³, Gilbert damping factor $\alpha = 0.05$, nonadiabaticity factor $\xi = 0.05$, and spin polarization of P = 0.7. Simulations are done at 0 K.

B. Neural Network and Classification Task

To quantify the utility of edgy-relaxed behavior in an ANN, a single-layer neural network (perceptron) utilizing the edgy-relaxed DW-MTJs as output neurons is constructed. The task selected is the classification of handwritten digits using the Optdigits dataset, a reduced-resolution version of the Modified National Institute of Standards and Technology (MNIST) handwritten digits dataset [Dua 2019]. To test the hypothesis that edgy-relaxed neurons excel in applications with datasets that have locality, a randomization scheme is devised. A test set of 100 images is sorted by digit into groups of 10. The completely sorted set is treated to have a degree of randomness of 0. Randomness is introduced by randomly selecting n images per digit group and swapping the images with a random counterpart drawn from the entire test set. The degree of randomness increases with n until n = 9, where the dataset is fully shuffled.

The construction of the perceptron is tailored for the classification of the Optdigits set. A set of 64 input neurons translate the pixel data into proportional voltage impulses. A network of 64×10 synapses is pretrained using 900 images from the Optdigits set and treated as perfect weights. The ten output neurons are simulated using an analytical model, where the index of the first neuron that fires is the classification of the image. The baseline neuron classification accuracy of 87% and completion time of the test set of 1.14 μs were determined using ten DW-MTJ output neurons. After classification of an image, the baseline neurons are hard reset using a 10 ns long current pulse. The reset circuitry is assumed to send minimum reset pulses of 10 ns duration for feasible implementation. The accuracy achieved is the theoretical accuracy possible for the pretrained synapse array on the input data, independent of the magnetic devices.

C. Analytical DW-MTJ Neuron Model

To evaluate the performance of edgy-relaxed DW-MTJ neurons, an analytical model is used to simulate the output neurons of the perceptron. A one-dimensional solution of DW motion is used as described by Beach [2008]. Due to the observation that the DW in the shape-anisotropy-driven soft reset case is in precession, the velocity of the DW in Walker breakdown regime is the following:

$$\bar{v} = \alpha \gamma \Delta H_{\text{eff}} + \frac{g\mu_B P}{2eM_{sqt}} j \tag{1}$$

where γ is the gyromagnetic ratio, Δ is the width of the DW, $H_{\rm eff}$ is the effective external magnetic field, g is the Landé factor, μ_B is the Bohr magneton, e is electron charge, and j is current density applied in the $-\hat{x}$. The effect of the sloped shape of the DW is approximated to have the effect of a constant external field. This assumption is accurate when the DW-MTJ neuron has a slight exponential curve to the DW track instead of a straight slope [Brigner 2020]. However, from the relaxation in DW position seen in Fig. 3, this is assumed to be a sufficient approximation for the device depicted in Fig. 2(a). $H_{\rm eff}$ due to slope is calculated by fitting (1) to DW relaxation in a micromagnetics model for each slope. The physical dimensions of the simulated analytical neurons are approximated to be the same as that of the device simulated in Section II-A. For the cases of external field-driven and current-driven soft reset cases, the DW remains in the Néel configuration due to the straight track. As a result, the expression

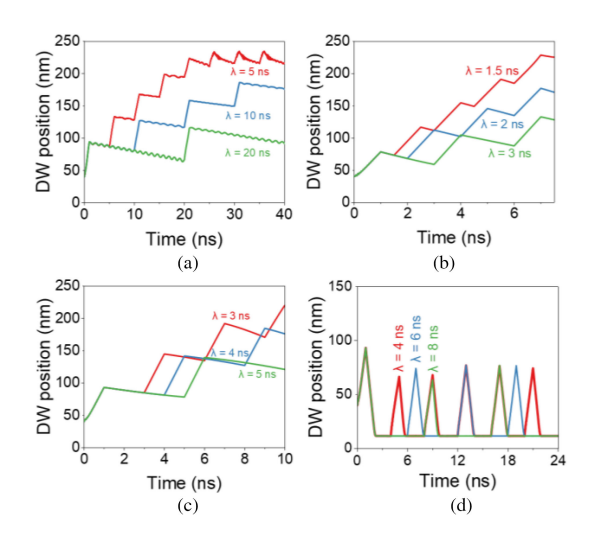


Fig. 3. DW position as a function of time due to repeated impulses for varying periods of time for soft reset methods of (a) shape anisotropy, (b) external field, (c) current, and (d) hard current reset as reference.

for DW velocity is for a DW in the non-Walker breakdown regime

$$\bar{v} = \frac{\gamma \Delta H_{\text{eff}}}{\alpha} + \frac{g\mu_B P}{2eM_{sat}} j \tag{2}$$

where the external field is represented by $H_{\rm eff}$ and the reset current is reflected in a change in j. The velocity of the DW is calculated at each timestep based on input current density and effective field. The new position is then calculated relative to the DW position at the previous timestep. A fixed timestep of 0.2 ps was used for the simulation. The fully relaxed position of the DW is set to be x=25 nm due to the inclusion of 10 nm fixed magnetization regions at the ends of the device and the approximate width of the DW.

III. RESULTS

A. Single-Device Edgy-Relaxed Behavior

Fig. 3 shows the inherent edgy-relaxed behavior of a single DW-MTJ neuron for shape-driven, field-driven, and current-driven reset methods. Here, using the micromagnetic model in Section II-A, an 80 μA pulse with 1 ns duration is applied for electron flow from IN to CLK with periods (λ) of varying length in red, blue, and green in increasing order. The DW position versus time plot shows the periods of integration during the pulse duration, when the DW position increases as it moves right toward the output MTJ, as well as periods of leaking after the current pulse is removed and the DW moves back toward the left of the FM track. After, for example, 40 ns in Fig. 3(a), the DW stimulated every 5 ns is farthest along the track, followed by 10 ns period and 20 ns period, respectively. Due to this, the neuron stimulated every 5 ns has the lowest firing threshold since it remains closer to the output MTJ, whereas the neuron stimulated every 20 ns has the highest firing threshold. Similar behavior is observed for the field-driven and current-driven reset methods in Fig. 3(b) and (c). This demonstrates that by modulating a soft reset, a DW-MTJ neuron can produce inherent behavior analogous to biological edgy-relaxed neurons. This contrasts with the hard reset shown in Fig. 3(d), where there is no difference in firing threshold between the three neurons.

DW dynamics at finite temperature are not significantly different, with the only difference being temperature noise introduced to the DW position measurement.

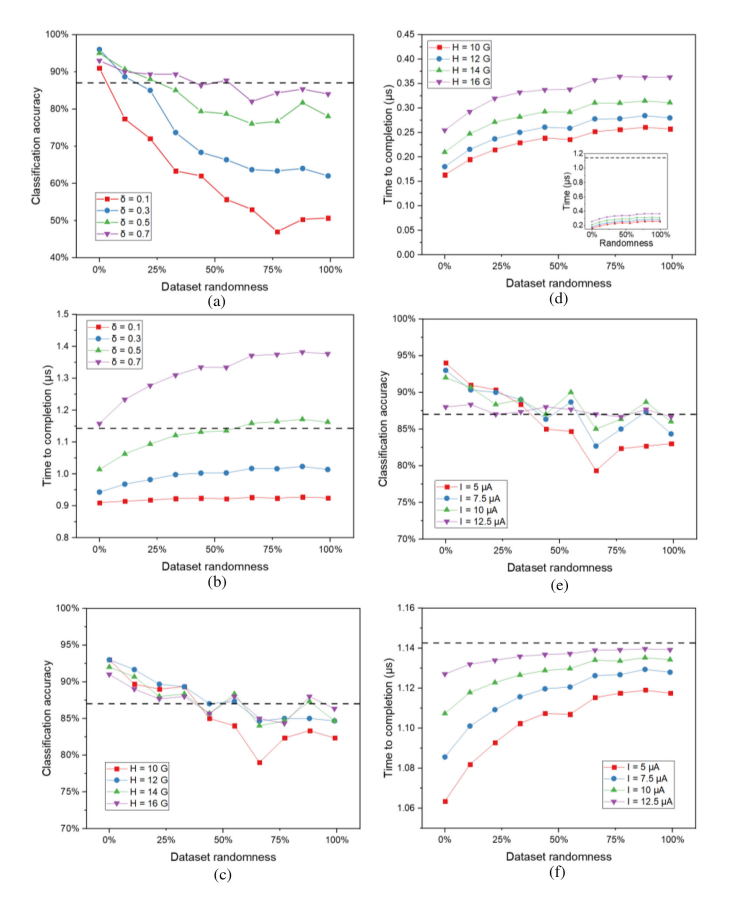


Fig. 4. Classification accuracy and completion time as a function of dataset randomness for varying (a), (b) device slopes δ , (c), (d) external magnetic fields H, and (e), (f) reset current amplitudes I. The baseline network classification accuracy of 87% and completion time of 1.14 μ s are shown as black dashed lines [inset for (d)].

B. Shape-Anisotropy-Driven Soft Reset

The utility of the edgy-relaxed behavior in DW-MTJ neurons in ANNs is addressed in this and subsequent sections for the different possible leaking methods. For shape-anisotropy-driven leaking DW-MTJs, output neurons with varying slopes of $\delta = \frac{W_2 - W_1}{L} = 0.1, 0.3,$ 0.5, and 0.7 are used to classify datasets of variable randomization using the analytical model of (1) and the crossbar array described in Section II-B. Because a racetrack with a larger width carries a current density penalty, we set $W_1 = 0$ nm to obtain competitive results, i.e., a triangular track. Because the leaking effect of shape anisotropy is relatively weak for tracks with physically reasonable slopes, a rest with a period of 9 ns is implemented after each classification to allow soft reset of the DW to reduce classification errors otherwise seen in higher randomness datasets. From the result in Fig. 4(a), for all geometries, there is enhanced classification accuracy for datasets with a relatively low degree of randomness. This improvement over the baseline is due to the repetition of presented images in each subgroup, a short-term learned repetition due to the edgy-relaxed neuron. The classification accuracy of a completely random dataset is also significantly increased with greater leak strength, at 50.67% for $\delta = 0.1$ versus 84.00% for $\delta = 0.7$, similar to the baseline network. However, this geometry results in a significant time penalty.

Fig. 4(b) depicts the total classification time of the test set. For all geometries, the greatest reduction in completion time results when

the edgy-relaxed neuron is applied to a nonrandom dataset and the completion time generally increases with increasing randomness. Additionally, the completion time increases with device slope due to the increased leaking effect along with the greater penalty to current density as the DW approaches the wider end of the device.

C. Magnetic-Field-Driven Soft Reset

External magnetic fields of H=10, 12, 14, and 16 G are applied in $-\hat{z}$ on output neurons with rectangular dimensions 50 nm wide \times 250 nm long \times 1.5 nm thick and implemented in the ANN from Section II-C using (2). The range of magnetic field strengths was chosen to be achievable values for a permanent magnet in proximity to the DW-MTJ neuron that could be engineered near the device or into the thin film stack. A rest with a period of 2 ns is implemented after each classification to allow a soft reset of the DW.

In Fig. 4(c), similar to the shape-based leaking, there is an enhancement in classification accuracy for nonrandom datasets and there is less accuracy penalty for highly randomized datasets than for the shape-anisotropy-driven case. It is also observed that as field strength increases, the more classification accuracy converges to the performance of the baseline neuron. Due to field-induced DW leak strength, there is a significant reduction in completion time, shown in Fig. 4(d). The completion time increases with dataset randomness and field strength, though all results are well below the completion time of the baseline neuron.

D. Current-Driven Soft Reset

The effect of a current-delivered soft reset without a leaking mechanism is studied by applying reset currents $I_{\text{reset}} = 5, 7.5, 10$, and $12.5 \,\mu\text{A}$ to DW-MTJ neurons with rectangular dimensions. The self-imposed limitation of a minimum 10 ns duration reset pulse is also applied in this case.

Fig. 4(e) shows that like the other methods discussed, a current-driven soft reset also enhances classification accuracy for nonrandom datasets over that of the baseline neuron. This holds until around 30% randomness. In general, the greater the magnitude of the reset current pulse, the more the classification accuracy converges to the result of the baseline neuron. For the $I_{\rm reset}=12.5~\mu{\rm A}$ case, the reset current pulse is close enough to a hard reset that the resulting trend is converging with the baseline neuron result and the enhancement to classification accuracy for the datasets with locality is largely lost.

From Fig. 4(f), it can be seen that there is an improvement in completion time for all reset current amplitudes, though there is no result that has a greater than 10% reduction. This is likely due to the limitation that the reset signal must have a minimum of 10 ns pulse duration. Though variation is not very large, the completion time generally increases with dataset randomness and reset current amplitude.

E. Practical Application Considerations

In addition to accuracy and speed, factors like area, current efficiency, fabrication difficult, and scalability are important for the experimental realization of edgy-relaxed behavior in DW-MTJ neurons. Table 1 presents a performance metric comparison between the soft reset methods described in this letter.

In terms of area, since shape-driven reset is only dependent on the lithographically defined free layer; the footprint is relatively small. This can also be the case for field-driven reset since the external

Table 1. Comparison of Shape Anisotropy, External Field, and Current Implementations of Edgy-Relaxed Behavior for Various Performance Metrics.

	Shape	Field	Current
Speed	Low	High	Medium
Accuracy	Medium	High	High
Area	Low	Low*	High
Current efficiency	Low	High	High
Fabrication difficulty	Low	High	Medium
Scalability	Low	Medium	High
Reconfigurability	No	Yes**	Yes

^(*) Area is low for external field due to magnetic layer in the stack. (**) This is only the case for external field due to circuitry.

magnetic field can be due to a layer engineered into the device stack. However, if this magnetic field is induced due to circuitry, the area cost is larger, similar to current-driven soft reset.

For current efficiency, shape-driven reset loses out to the other options since DW velocity relies on current density, and a wider DW requires a larger amount of current to propagate. Therefore, to attain the same performance as the baseline DW-MTJ neuron, a larger current is required for the integration. There is no significant current efficiency cost for the other types described.

Fabrication difficulty of field-driven edgy-relaxed DW-MTJs is high due to strong leaking effect for relatively small fields. As a result, induced field either due to a magnetic layer in the device stack or external circuitry must be carefully tuned, which can also lead to scaling difficulties. Shape-driven edgy-relaxed neurons can be lithographically defined, leading to a relatively easy fabrication process. However, the sloped design is a barrier for scalability. The difficulty in fabrication for current-driven reset comes from the required external circuitry, but CMOS is already well-scaled, and current efficiency increases as the DW-MTJ device becomes narrower, leading to better scalability than the other options.

A factor that can lead to extended functionality is the reconfigurability of edgy-relaxed strength. In the case of current-driven reset, the reset current can be designed to change dynamically based on the data received by the ANN, i.e., an algorithm can be used to determine the prevalence of repeated data and adjust the strength of edgy-relaxed behavior accordingly. This can also be implemented in field-driven reset, though this only applies to magnetic field applied through external circuitry. Since shape-driven edgy-relaxed neurons are lithographically defined, this would not be an option.

IV. CONCLUSION

Biological neurons have an adaptive edgy-relaxed transition behavior when repeatedly stimulated, leading to a reduced threshold for the action potential. This letter demonstrates ways this behavior can be implemented intrinsically in a DW-MTJ LIF neuron by exploiting magnetic properties of shape anisotropy and external magnetic field to manipulate DW movement. An additional method of modulating the reset pulse is also developed and can be widely applied to other types of analog neuron devices. By modulating soft reset, the classification accuracy on a dataset with repeated data can be improved significantly due to the intrinsic short-term memory of edgy-relaxed behavior. Additionally, there is a significant improvement in classification time for external field implementation and a slight improvement for reset

pulse modulation. This letter establishes ways that unique magnetic properties can be utilized to implement edgy-relaxed behavior in a DW-MTJ neuron, supported by micromagnetics and analytical modeling along with the discussion on various performance metrics. These results can lead to ANNs that can be adapted to different types of expected datasets through modification of neuron device behavior.

ACKNOWLEDGMENT

This work was supported in part by the National Science Foundation CAREER under Award 1940788, in part by the Sandia National Laboratories Laboratory Directed Research and Development Program, and in part by the Computing Resources from the Texas Advanced Computing Center at the University of Texas at Austin. This letter describes objective technical results and analysis. Any subjective views or opinions that might be expressed in this letter do not necessarily represent the views of the U.S. Department of Energy or the U.S. Government. Sandia National Laboratories is a multimission laboratory managed and operated by NTESS, LLC, a wholly owned subsidiary of Honeywell International Inc., for the U.S. Department of Energy's National Nuclear Security Administration under Contract DE-NA0003525.

REFERENCES

Alamdar M, Leonard T, Cui C, Rimal B P, Xue L, Akinola O G, Xiao T P, Friedman J S, Bennett C H, Marinella M J, Incorvia J A C (2021), "Domain wall-magnetic tunnel junction spin orbit torque devices and circuits for in-memory computing," *Appl. Phys. Lett.*, vol. 118, 112401, doi: 10.1063/5.0038521.

Beach G, Tsoi M, Ersksine J (2008), "Current-induced domain wall motion," J. Magn. Magn. Mater., vol. 320, pp. 1272–1281, doi: 10.1016/j.jmmm.2007.12.021.

Bean B P (2007), "The action potential in mammalian central neurons," Nature Rev. Neurosci., vol. 8, pp. 451–465, doi: 10.1038/nrn2148.

Brigner W H, Hassan N, Hu X, Bennett C H, Garcia-Sanchez F, Cui C, Velasquez A, Marinella M J, Incorvia J A C, Friedman J S (2020), "Domain wall leaky integrate-andfire neurons with shape-based configurable activation functions," arXiv:2011.06075.

Brigner W H, Hassan N, Jiang-Wei L, Hu X, Saha D, Bennett C H, Marinella M J, Incorvia J A C, Garcia-Sanchez F, Friedman J S (2019), "Shape-based magnetic domain wall drift for an artificial spintronic leaky integrate-and-fire neuron," *IEEE Trans. Electron Devices*, vol. 66, pp. 4970–4975, doi: 10.1109/TED.2019.2938952.

Burkitt A N (2006), "A review of the integrate-and-fire neuron model: I. Homogeneous synaptic input," Biol. Cybern., vol. 95, pp. 1–19, doi: 10.1007/s00422-006-0068-6.

Cui C, Akinola O G, Hassan N, Bennett C H, Marinella M J, Friedman J S, Incorvia J A C (2020), "Maximized lateral inhibition in paired magnetic domain wall racetracks for neuromorphic computing," *IOP Nanotechnol.*, vol. 31, 294001, doi: 10.1088/1361-6528/ab86e8.

Currivan J A, Jang Y, Mascaro M D, Baldo M A, Ross C A (2012), "Low energy magnetic domain wall logic in short, narrow, ferromagnetic wires," *IEEE Magn. Lett.*, vol. 3, 3000104, doi: 10.1109/LMAG.2012.2188621.

Currivan-Incorvia J, Siddiqui S, Dutta S, Evarts E R, Zhang J, Bono D, Ross C A, Baldo M A (2016), "Logic circuit prototypes for three-terminal magnetic tunnel junctions with mobile domain walls," *Nature Commun.*, vol. 7, 10275, doi: 10.1038/ncomms10275.

Dua D, Graff C (2019), "UCI Machine Learning Repository," School Inf. Comput. Sci., Univ. California, Irvine, CA, USA. [Online]. Available: http://archive.ics.uci.edu/ml Furber S (2016), "Large-scale neuromorphic computing systems," J. Neural Eng., vol. 13, 051001, doi: 10.1088/1741-2560/13/5/051001.

Hassan N, Hu X, Jiang-Wei L, Brigner W H, Akinola O G, Garcia-Sanchez F, Pasquale M, Bennett C H, Incorvia J A C, Friedman J S (2018), "Magnetic domain wall neuron with lateral inhibition," *J. Appl. Phys.*, vol. 124, 152127, doi: 10.1063/1.5042452.

Llinás R R (1988), "The intrinsic electrophysiological properties of mammalian neurons: Insights into central nervous system function," *Science*, vol. 242, pp. 1654–1664, doi: 10.1126/science.3059497.

Nahmias M A, Shastri B J, Tait A N, Prucnal P R (2013), "A leaky integrate-and-fire laser neuron for ultrafast cognitive computing," *IEEE J. Sel. Topics Quantum Electron.*, vol. 19, 1800212, doi: 10.1109/JSTQE.2013.2257700.

Sengupta A, Shim Y, Roy K (2016), "Proposal for an all-spin artificial neural net-work: Emulating neural and synaptic functionalities through domain wall motion in ferromagnets," *IEEE Trans. Biomed. Circuits Syst.*, vol. 10, pp. 1152–1160, doi: 10.1109/TBCAS.2016.2525823.

Sharad M, Augustine C, Panagopoulos G, Roy K (2012), "Spin-based neuron model with domain-wall magnets as synapse," *IEEE Trans. Nanotechnol.*, vol. 11, pp. 843–853, doi: 10.1109/TNANO.2012.2202125.

Vansteenkiste A, Leliaert J, Dvornik M, Helsen M, Garcia-Sanchez F, Waeyenberge B V (2014), "The design and verification of MuMax3," AIP Adv., vol. 4, 107133, doi: 10.1063/1.4899186.

Wulf W A, McKee S A (1995), "Hitting the memory wall: Implications of the obvious," SIGARCH Comput. Archit. News, vol. 23, pp. 20–24, doi: 10.1145/216585.216588.